ELSEVIER

Nuclear Instruments and Methods in Physics Research B 184 (2001) 361–370

NIM B
Beam Interactions with Materials & Atoms

www.elsevier.com/locate/nimb

Structural characterization of high-dose $C^+ + N^+$ ion-implanted (1 1 1) Si

L. Barbadillo [a,*], M.J. Hernández [a], M. Cervera [a], P. Rodríguez [a], J. Piqueras [a], S.I. Molina [b], F.M. Morales [b], D. Araújo [b]

[a] *Laboratorio de Microelectrónica, Departamento de Física Aplicada, Facultad de Ciencas, C-XI 100, Universidad Autónoma de Madrid, Cantoblanco, 28049 Madrid, Spain*

[b] *Departamento de Ciencia de los Materiales e Ingeniería Metalúrgica y Química Inorgánica, Universidad de Cádiz, Apdo. 40, 11510 Puerto Real (Cádiz), Spain*

Received 3 August 2000; received in revised form 3 July 2001

Abstract

(1 1 1) silicon wafers were implanted with high ion doses of C^+, N^+ and $C^+ + N^+$, from 1×10^{16} to 6.7×10^{17} cm^{-2}, well over the amorphization dose. For the largest dose, the mean impurity concentration in the implanted region (of about 1000 Å) at 30 keV is expected to be similar to the Si atom density. Silicon nitride and silicon carbide formation is detected in the as-implanted samples. After annealing at 1200 °C a trend to segregation of Si_3N_4 and SiC in separated layers is observed, and a polycrystalline Si overlayer is formed. © 2001 Elsevier Science B.V. All rights reserved.

1. Introduction

The growth of high-quality epitaxial films on lattice-mismatched substrates has proved to be extremely useful in the fabrication of high-performance semiconductor devices. The induced elastic strain allows tailoring the electronic properties of the device to specific requirements. Unfortunately the film thickness is limited to below a critical thickness, over which films begin to degrade. Their potential applications in heterojunction bipolar transistors have caused a great research effort in methods to achieve strain relaxation, which would allow larger thicknesses without degradation. The utilization of compliant substrates is one of the most common approaches. With the appearance of compliant substrates, where the substrate becomes mechanically flexible to comply with the lattice of the epitaxial layer, this limitation has been avoided.

Ion implantation is a powerful method for modifying the near-surface properties of materials. A promising application for ion implantation is the formation of silicon-on-insulator (SOI) structures, which have also been used as compliant substrates [1–4]. In this case, the thin silicon overlayer will absorb stress, enabling the growth of

* Corresponding author. Tel.: +34-91-397-8607; fax: +34-91-397-4895.

E-mail address: lucia.barbadillo@uam.es (L. Barbadillo).

0168-583X/01/$ - see front matter © 2001 Elsevier Science B.V. All rights reserved.
PII: S0168-583X(01)00783-2

thicker layers without degradation [5,6]. Additionally, buried SiN_x films find a wide range of applications in microelectronics, not only as SOI structures [7–10], but also as etch-stop [11,12] and selective oxidation masks [13]. SiC layers generated by high-dose implantation could be useful as buffer layers for crystalline GaN growth on Si, because the lattice mismatch between β-GaN and SiC is 3%, while that between β-GaN and Si is about 17% [14].

Carbon implantation in SOI structures has been reported to result in preferential carbon migration to the silicon/insulator interfaces [15], where continuous carbide layers in epitaxial relation with the silicon matrix can be achieved.

Carbon and nitrogen co-implantation could be applied to obtain compliant substrates, allowing a reduction of the lattice constant in the silicon overlayer because of their covalent radii, both smaller than the one of the silicon (carbon 0.77 Å and nitrogen 0.75 Å versus 1.11 Å of silicon).

Furthermore, because of the similarity between the basic structures of C_3N_4 and Si_3N_4, both could be miscible giving rise to SiCN alloys with potential applications in microelectronics and hard coating technologies. The formation of some middle state $Si_xC_yN_z$, different from SiC and Si_3N_4, by nitrogen implantation in SiC has been previously reported [16,17]. Later, electron cyclotron resonance (ECR) CVD [18,19] and microwave-enhanced CVD [20] have been used to synthesize SiCN layers. In addition, SiCN appears to be a direct-wide-band-gap semiconductor with potential optoelectronic applications in the blue or ultraviolet region [20].

The aim of the present work is to study the properties of the layers formed by low-energy carbon and nitrogen implantation into silicon, and the effects of post-annealing processes.

2. Experimental

Implantation of C^+ and/or N^+ was carried out at 30 keV in a modified Varian Extrion ion implanter using a gas mixture of $CO + N_2$ as ion source. In the co-implantated samples the implantation of nitrogen was performed in first place. The C^+ and N^+ ion current densities were about 1.5 and 3 μA/cm^2, respectively. Projected ranges of both species, at this energy, are close to 1000 Å, as predicted by the SRIM [21] program. Both-sides polished N-type float-zone (FZ) (1 1 1) silicon wafers, with resistivity over 50 Ω cm and oxygen content below 0.3 ppm, were implanted with different doses (1×10^{16}, 1×10^{17} and 6.7×10^{17} cm^{-2} for $^{14}N^+$ and 1×10^{16}, 1×10^{17} and 5×10^{17} cm^{-2} for $^{12}C^+$). All of them were well over the critical amorphization dose, of about 10^{15} cm^{-2} for these ions at 30 keV in silicon.

The highest dose was chosen to obtain a concentration of the implanted ions at a depth of about 0.1 μm similar to the bulk silicon density, 5×10^{22} cm^{-3}.

During the process the sample holder was maintained at room temperature by means of a closed-cycle circuit of coolant, in order to avoid self-annealing effects. With the used ion current densities the mean temperature increase induced by the beam does not exceed 150 °C, even if the sample holder was uncooled.

Afterwards, the samples were annealed in pure nitrogen atmosphere to achieve a good-crystalline-quality Si overlayer and to promote the activation and/or chemical reaction of the implanted ions. Two of the samples of each dose were rapid thermal annealing (RTA) annealed in nitrogen for 1 min at 600 and 1200 °C and two additional pieces furnace annealed for 3 h at 1200 °C.

The structural changes originated in Si by N^+ and C^+ implantation have been studied by conventional transmission electron microscopy (TEM), high-resolution electron microscopy (HREM) and selected-area electron diffraction (SAED). Conventional TEM work was carried out in a Jeol 1200 EX while a Jeol 2000 EX was operated for HREM studies. SAED analysis was performed using both transmission electron microscopes. Electron diffraction patterns and HREM image analysis were carried out using Digital Micrograph and Semper softwares. All studies were carried out after preparing cross-section (X) specimens by mechanical thinning and further Ar^+ ion milling at 4.5 kV.

The crystalline quality of the Si overlayer was also checked by means of high-resolution X-ray

diffraction (HRXRD) measurements of the implanted samples annealed at higher temperatures, both in RTA and conventional furnace, performed in a Siemens D-5000 diffractometer. The Cu-Kα radiation at 1.54 Å was used as the source for diffraction.

Fourier transform infrared (FTIR) spectra in transmission mode were collected with a Bruker IFS-66V spectrometer. This technique was used to identify the vibrational modes of the different bonds present in all the samples and, thus, to follow the reaction between the implanted ions and the silicon matrix.

Spectroscopic ellipsometry (SE) measurements of the samples were performed in a Uvisel Jobin–Yvon spectrometer between 1.5 and 4.5 eV. Using the qualitative composition deduced from FTIR spectra, it was possible to deduce the layer structure and thickness, by fitting the SE measurements to adequate models.

3. Results

3.1. TEM observations

XTEM images of the sample implanted with the highest doses of C^+ (5×10^{17} cm^{-2}) and N^+ (6.7×10^{17} cm^2) and annealed at 1200 °C for 3 h show three well-defined layers near the silicon surface. Fig. 1 shows an XTEM image where these layers are labeled as layers 1 (the deepest one), 2 and 3 (the closest to the sample surface). Average thickness measured from XTEM images is 22 nm for layer 1, 85 nm for layer 2 and 82 nm for layer 3.

SAED pattern of Fig. 2 is a typical diagram registered from layers 1, 2 and 3. This pattern contains (i) the main spots of a characteristic electron diffraction pattern of monocrystalline Si along [1 1 0]; (ii) spots arranged around circumferences due to polycrystalline Si (planes {1 1 1}, {2 2 0} and {1 1 3}); and (iii) spots X_1, X_2, X_3 and X_4 that do not correspond to silicon. Spot X_1 corresponds to a lattice spacing of 2.152 ± 0.039 Å, X_2 to 4.283 ± 0.061 Å, X_3 to 4.554 ± 0.070 Å and X_4 to 2.253 ± 0.032 Å. Considering lattice spacing of α-Si_3N_4, β-Si_3N_4, 2H–SiC, 4H–SiC and 6H–SiC, X_1 and X_3 cannot be assigned to a single phase. On the contrary, X_2 and X_4 are assigned to lattice spacings of α-Si_3N_4. X_2 is assigned to lattice spacing of 4.313 Å, which corresponds to planes (1 −1 1), (0 1 1), (1 0 1), (−1 1 1), (0 −1 1) and (−1 0 1), and X_4 to 2.277 Å, which corresponds to planes (−1 −1 2), (2 −1 2), (−1 2 2), (1 1 2), (−2 1 2) and (1 −2 2).

Layer 1 consists only of monocrystalline Si oriented with its [1 1 0] direction parallel to the

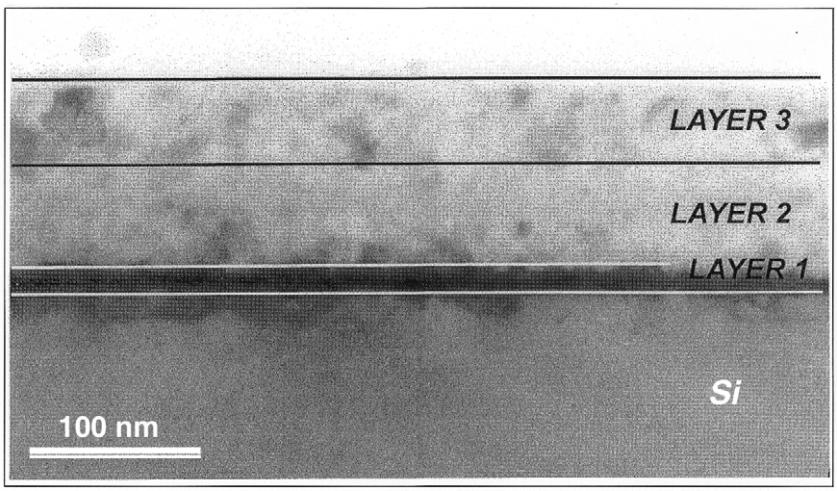

Fig. 1. Bright field XTEM image of layers formed in the C^+- and N^+-implanted sample (5×10^{17} cm^{-2} of C^+ and 6.7×10^{17} cm^{-2} of N^+) furnace-annealed at 1200 °C for 3 h.

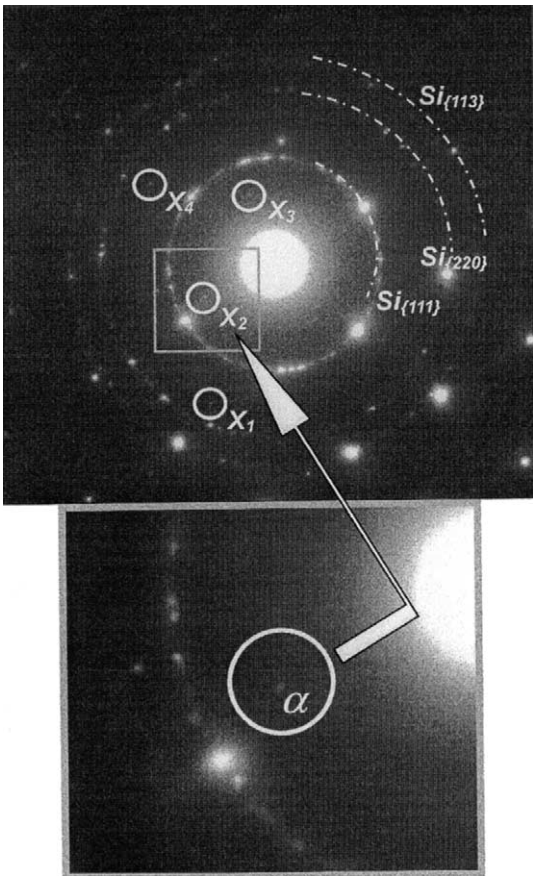

Fig. 2. SAED pattern registered from layers 1, 2 and 3 of the C^+ and N^+-implanted sample. Spots X_1, X_2, X_3 and X_4 do not correspond to Si. Spots X_2 and X_4 are due to α-Si_3N_4.

electron beam. However, this layer presents a contrast darker than Si non-affected by implantation, located below layer 1. The interface between layer 1 and the deepest non-affected Si substrate is well defined though occasionally the dark contrast of layer 1 is observed to penetrate up to 20 nm in the Si substrate, as is visible in XTEM image of Fig. 1.

SAED patterns, as that of Fig. 2, permit us to deduce that layers 2 and 3 must also consist mostly of Si. Fig. 3(a) shows a HREM image where crystalline inclusions are visible in the amorphous matrix of layer 2. Careful inspection of XTEM images of layer 2 reveals differences between the regions closest to layer 3 and layer 1. In the neighborhood of layer 1 a larger abundance of

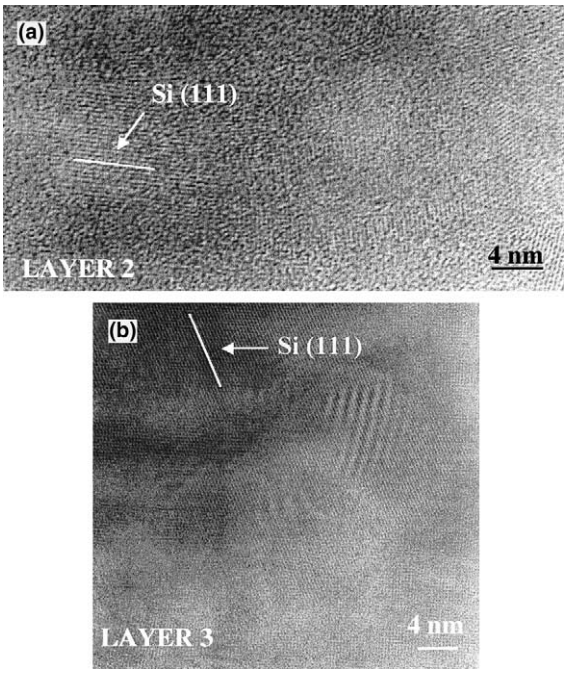

Fig. 3. HREM images from layers 2 (a) and 3 (b) of the C^+- and N^+-implanted sample.

crystalline inclusions has been observed. On the other hand, Fig. 3(b) shows a HREM image where the polycrystalline nature of layer 3 is evident and where amorphous material is almost inexistent. (1 1 1) Si planes are the most frequently observed in these layers and they have been marked on both HREM images. HREM shows, therefore, that layer 2 is an amorphous layer with crystalline inclusions while layer 3 is mostly a polycrystal.

α-Si_3N_4 phase detected from SAED pattern of Fig. 2 must be included in these semicrystallized layers 2 and 3. However, the presence of other phases cannot be discarded because spots X_1 and X_3 are not due to Si crystal.

3.2. X-ray diffraction

HRXRD measurements were performed in a Siemens D-5000 diffractometer, using the Cu-Kα radiation. XRD rocking curves of the samples implanted with 6.7×10^{17} cm^{-2} N^+ and 5×10^{17} cm^{-2} C^+ and annealed at 1200 °C around the (1 1 1) Si reflection are shown in Figs. 4 and 5.

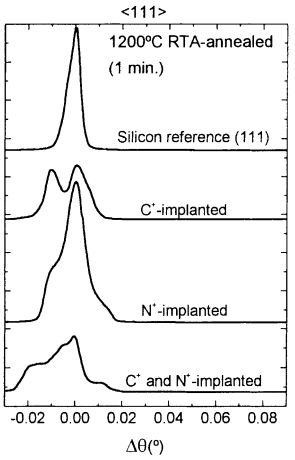

Fig. 4. Rocking curves of 1200 °C RTA-annealed samples implanted with 5×10^{17} cm^{-2} of C^+ and 6.7×10^{17} cm^{-2} of N^+.

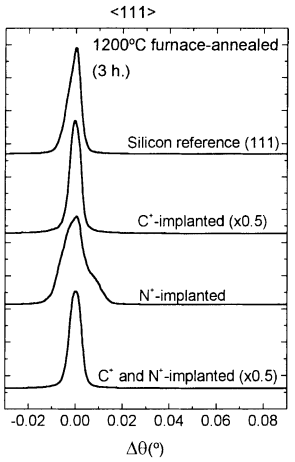

Fig. 5. Rocking curves of 1200 °C furnace-annealed samples implanted with 5×10^{17} cm^{-2} of C^+ and 6.5×10^{17} cm^{-2} of N^+. (The intensity of the curves of the samples implanted with C^+ and $N^+ + C^+$ has been corrected by a factor 0.5.)

Unprocessed Si wafers were also measured as reference.

In the RTA-annealed N^+ implanted sample the main peak, corresponding to the substrate, shows two shoulders (see Fig. 4). The one at larger diffraction angles is usually attributed to the slight lattice parameter reduction due to substitutional N atoms. A second shoulder, on the left side, may indicate disorder in the outermost layers. However, an alternative explanation is an increase of the lattice parameter at the maximum depth of the implantation, due to the concentration of interstitial N atoms, much higher than the solubility limit of nitrogen in silicon.

In the N^+-implanted sample after furnace annealing (see Fig. 5), the left-hand shoulder is hardly distinguished. Probably, after such a prolonged annealing, most of the N segregated in a buried layer, mainly of Si_3N_4, reducing considerably the disorder in the silicon overlayer. It presents only a slight asymmetry at the right-hand side, also due to a reduction of the lattice constant in the near-surface region. Nevertheless, the appearance of the peak indicates that diffusion of N atoms allows an improved crystallinity of the regrown layers, above and below the Si_3N_4 buried layer.

The rocking curve of the RTA-annealed C^+-implanted sample (see Fig. 4(b)) shows a second peak on the left of the main one corresponding to a slight expansion ($\Delta d \cong 0.08\%$) of the lattice. In the furnace-annealed sample (see Fig. 5(b)) this left peak disappears. This means that the diffusion of C atoms might either promote their incorporation into substitutional sites or the segregation of SiC clusters, reducing by this way the interstitial concentration. This results in a relaxation of the silicon overlayer improving its crystalline quality, as demonstrated by the main peak, significantly narrower and higher than the reference peak.

The $N^+ + C^+$-implanted samples exhibit rocking curves quite similar to those shown for the N^+-implanted samples. In the curve of the RTA-annealed sample (see Fig. 4(d)), two shoulders around the main peak can be observed. The one on the right side is related to a lattice parameter reduction, caused by substitutional impurity atoms, and the one on the left may indicate disorder in the outermost layers. As in the C^+-implanted sample, diffusion processes induced by the longer furnace annealing again allow the recovery of the silicon structure, reaching such an optimum crystalline structure as in the C^+-implanted sample.

Even though SAED results confirmed the presence of crystalline clusters of Si_3N_4 and suggested the possible presence of SiC clusters in the furnace-annealed samples, no peaks due to materials different than c-Si were detected in any of the

obtained XRD patterns. This indicates that other crystalline phases are present only at slight concentrations, randomly oriented, or that the contribution to the XRD satellite peaks and shoulders are mainly due to regions close to the substrate where Si is the most abundant species.

3.3. FTIR measurements

The IR spectra in transmission mode of some samples implanted with N^+ (6.7×10^{17} cm^{-2}) and C^+ (5×10^{17} cm^{-2}) are presented in Fig. 6: before annealing (Fig. 6(a)), after 1200 °C RTA annealing (Fig. 6(b)) and 1200 °C furnace annealing (Fig. 6(c)). An unimplanted silicon wafer is used as reference, but no baseline corrections were done. In some cases the anti-reflecting behavior of the implanted layer leads to an overestimation of the sample transmittance, especially apparent in the lowest-dose samples due to their low absorption. Since not too many significant differences were found between the spectra of samples implanted with different doses, only some typical cases are presented here (Fig. 6).

The spectrum of the non-annealed C^+-implanted sample (Fig. 6(a)) displays a very broad band peaking at about 735 cm^{-1}. After the 1200 °C-RTA annealing (Fig. 6(b)) is shifted towards 818 cm^{-1} and becomes progressively narrower. Finally, after the 1200 °C-furnace annealing (Fig. 6(c)), the peak position is 820 cm^{-1} and the FWHM about 77 cm^{-1}. Similar results have been previously reported [22,23]. The wide band at around 735 cm^{-1} (Fig. 6(a)) has been ascribed to SiC bands in an amorphous environment [24]. The final FWHM, 77 cm^{-1}, is typical of single-crystal [24,25] microcrystalline SiC [26,27]. However the peak position is shifted towards larger wave numbers as compared with the standard, 780–800 cm^{-1}, frequency of the SiC band in a crystalline environment [25,28]. In carbon-implanted silicon, after high-temperature annealing, the Si–C stretching band has been reported to be from 795 cm^{-1} [29,30] up to 820 [23] or 830 cm^{-1} [22] depending on the implanted dose and annealing. The segregation of isolated SiC clusters inside the silicon matrix might be responsible for this anomalous SiC band frequency [22].

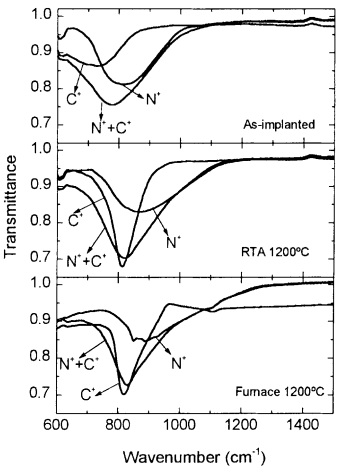

Fig. 6. FTIR spectra of the samples implanted with 5×10^{17} cm^{-2} of C^+ and 6.7×10^{17} cm^{-2} of N^+ (a) before annealing, (b) after 1200 °C RTA annealing, and (c) after 1200 °C furnace annealing.

In the C^+-implanted samples, the peak of substitutional C (605 cm^{-1}) [31] cannot be distinguished, as the Si–Si stretching band at 610 cm^{-1} probably masked it.

The spectrum of the N^+-as-implanted sample (Fig. 6(a)) displays a wide band centered at about 820 cm^{-1}. After the RTA annealing at 1200 °C (Fig. 6(b)) this band shifted to 880 cm^{-1} and apparently widens towards larger wave numbers. This apparent widening may be explained by the appearance of new phases, which have contributions in the larger wave number side of the 880 cm^{-1} band. In fact, regarding the IR spectrum of the same sample after a 3 h-1200 °C-furnace annealing, this band is even more shifted and presents certain structures on the top, peaking at 848, 885 and 928 cm^{-1}. The peak structure of the band looks similar to a mixture of α and β crystalline Si_3N_4 [32,33]. In this spectrum, certain bowing can also be observed in the region around 1000 cm^{-1}, probably due to free-carriers absorption produced by the donor behavior of nitrogen atoms in substitutional sites.

In the samples implanted with C^+ and N^+ after the 1200 °C-furnace annealing this bowing can be observed too. The three spectra of $C^+ + N^+$-implanted samples show a wide band, centered at

780 cm^{-1} for the as-implanted sample, at 825 for the 1200 °C-RTA-annealed and at 835 cm^{-1} for the 1200 °C-furnace-annealed sample. In all three cases the spectra look approximately like a sum of spectra of the samples implanted only with C^+ or N^+.

3.4. Spectroscopic ellipsometry

Spectroscopic ellipsometry measurements were performed between 1.5 and 4.5 eV using a Uvisel Jobin–Yvon ellipsometer, with an experimental accuracy in the ellipsometric angles, ψ and δ, better than 0.02°. The spectra measured in N^+-implanted (1 1 1) samples and multilayer structures obtained from their fittings are in excellent agreement with previous results in N^+-implanted (1 0 0) silicon [34]. This supports the quality and reliability of those results. It also indicates that the orientation has not a strong influence on the chemical composition and the optical properties of the layers.

It is possible to estimate the composition and the thickness of the resulting films by means of a conventional procedure [35]. It is based in a least-squares fitting done by fixing initial values and varying them to minimize the sum of the errors in the equations that relate the measured ellipsometric angles ψ and Δ and the optical properties of the films (refractive indexes and absorption coefficients) [36,37].

Using different theoretical approaches of the effective medium to simulate the optical properties of the films by changing the relative concentration of its components, this technique can be applied to the analysis of inhomogeneous films. In our case we have used only the two main approximations. The Maxwell–Garnett model (see for example [38]) is employed when the main component (a) can be considered as a "host" (h) for the others (over 75% in composition), and thus the dielectric constant of this main component is considered as dielectric constant of a host in which the other components are included ($\epsilon_h \approx \epsilon_a$). The Bruggeman model [38] is applied when components (a, b,...) are in similar proportions and allows to obtain the effective dielectric constant by considering as host, the effective medium itself ($\epsilon_h = \epsilon$).

The sensitivity of the technique is limited to the outer few thousands of angstroms, since the absorption constant, α, of silicon is between 10^3 and 10^5 cm^{-1} in the spectral range of measurements.

In all cases the pseudodielectric constant of the implanted samples may be fitted to a structure consisting in essentially three layers. A polysilicon overlayer on top and mostly crystalline silicon close to the substrate separated by a sort of transparent layer. As an example, Fig. 7 shows the SE spectrum of the $C^+ + N^+$-highest-dose-implanted sample after a 1200 °C-furnace annealing of 3 h. As can be seen the imaginary part of the dielectric constant displays a double-peaked structure rather similar to the spectrum of crystalline silicon (c-Si). The dielectric constant of crystalline silicon can be described in terms of the classical damped-harmonic-oscillator *model* (DHO), with two main contributions at the critical points, 3.5 and 4.2 eV. However, these peaks are less pronounced in our case than in c-Si. This structure is mainly due to the absorption in the polysilicon overlayer. Towards 2.2 and 2.8 eV a structure resembling the above one appears. This is caused by the inner Si layer close to the substrate. Because the separation between different layers is not clearly defined as demonstrated by TEM observations and, moreover, layer 2 is not homogenous, we have tried to simulate the pseudodielectric constant by a five-layers structure.

The best fitting corresponds to a structure, from top to bottom: layer 5 of about 70 Å of native

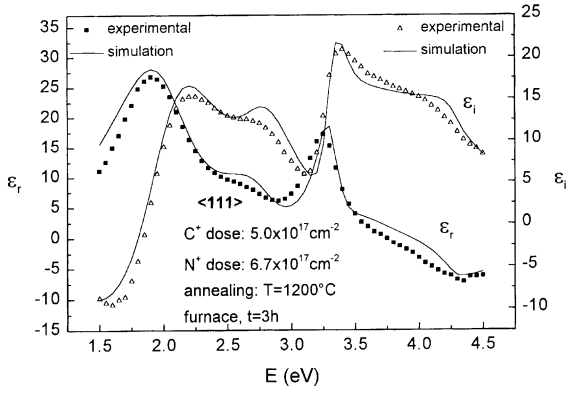

Fig. 7. Ellipsometry measurements of the 1200 °C furnace-annealed sample implanted with 5×10^{17} cm^{-2} of $C^+ + 6.7 \times 10^{17}$ cm^{-2} of N^+.

oxide, layer 4, with an approximate thickness of 465 Å and a high content of polycrystalline silicon (55% c-Si + 25% SiC + 20% amorphous silicon (a-Si)), a mostly Si_3N_4 layer 3 of 235 Å (85% Si_3N_4 + 11.5% SiC + 3.5% c-Si), a mostly SiC layer 2 of 660 Å (80% SiC + 13% a-Si + 7% c-Si) and, finally, close to the substrate an almost crystalline Si layer 1 of 520 Å (78% c-Si + 13% Si_3N_4 + 9% SiC). The amorphous silicon content is normally used to represent the disorder regions between crystalline grains. It should be noted that a one to one correspondence between layers observed by TEM and layers of the best SE fit cannot be met probably because composition and structure gradually change inside each layer, specially in the case of layers 2 and 3 of the SE fitting, that should correspond to the layer 2 observed by TEM. More accurate fittings could probably be obtained by increasing the number of layers and of components inside each layer. In any case, the overall thickness of the modified surface layers as estimated by SE spectra simulation, about 1950 Å, is in good agreement with that observed by TEM, about 1890 Å.

The outermost native oxide can be as well identified as a polycrystalline or rough layer at the surface. It is also possible to simulate it with a thin film of SiC that cannot be disregarded since other results show a certain superficial carbon piling-up [17].

4. Discussion

High-dose C^+, N^+ or $C^+ + N^+$ ion implantation at 30 keV leads to the formation of a surface region of about 1000 Å rich in the implanted species. The thickness of this region, measured both by TEM and SE, is in good agreement with the expected penetration depth estimated by the SRIM code. In the as-implanted samples, the formation of silicon carbide and silicon nitride phases has been observed by FTIR, even though no intentional heating of the substrates was provided. However, in view of the large widths of the observed IR bands, both SiC and SiN_x are in highly distorted or amorphous networks.

After high-temperature annealing, both carbon and nitrogen partially segregate giving rise to a layered structure in the near-surface region. This region consists, from top to bottom, of a polycrystalline Si overlayer (layer 3) with some inclusions of other crystalline phases. In the case of the $N^+ + C^+$-implanted sample, small clusters of α- and β-Si_3N_4, and hexagonal SiC have been detected. This overlayer may be simulated in SE fittings by 75% Si-rich polycrystalline region with inclusions of a more transparent material.

Below layer 3, a nearly amorphous region (layer 2) extends down to a crystalline Si region (layer 1). In this last layer a darker contrast is observed by TEM, probably due to a high N concentration in substitutional sites. The SE spectra may be simulated by a structure, which qualitatively agrees with that observed by TEM. Moreover, simulations of SE spectra indicate that composition inside each layer is not homogeneous, as suggested by TEM in case of layer 2. The inhomogeneous composition of layer 2 may be simulated in SE by using two sublayers, one of them Si_3N_4-rich and the other SiC-rich.

XRD rocking curves around the (1 1 1) Si direction show a single peak in the C^+ and $C^+ + N^+$-implanted samples after furnace annealing at 1200 °C for 3 h (see Fig. 5).

In the sample implanted with N^+, a small shoulder at the right side and a certain distortion in the left side are observed. The RTA-annealed samples exhibit some striking XRD rocking curves (Fig. 4). Further to the right-hand shoulders, left-hand shoulders are clearly seen. Moreover, in the C^+-implanted sample a clear satellite peak appeared. We believe that the right-hand side contribution may be due to the deepest region, layer 1, and indicates lattice contraction due to the high N and/or C concentration in substitutional sites. The shoulders and peaks at the left-hand side of the main peak indicate expansion of the network. This expansion of the lattice may be attributed to implanted atoms exceeding the solubility limit, which tend to be located in interstitial sites or to self-interstitials. This effect has been observed in C^+-implanted silicon at intermediate annealing temperatures. However, after high-temperature annealings, SiC clusters segregation tends to relax

the lattice with a reduction of the lattice expansion [22]. Probably layer 3 and, partly, layer 2 are responsible for these left-hand side contributions. However, we cannot disregard the rise of expansive stress in the (1 1 1) direction due to the formation of anisotropic structures, such as hexagonal crystalline phases.

5. Conclusions

High-dose C^+, N^+ and $C^+ + N^+$ ion implantations lead to the formation of silicon carbide and/or silicon nitride even if the implantation is done at room temperature. After annealing, a trend of C and N to segregate forming Si_3N_4 and SiC is demonstrated, allowing the recovery of the crystalline quality of the overlayer. Even when both impurities are implanted, silicon nitride and silicon carbide tend to segregate in separated layers. However, for the annealings at 1200 °C this separation seems to be uncompleted. The polycrystalline silicon overlayer, after the 1200 °C-3 h annealing, has still a small amorphous content and clusters different from Si. Higher temperature annealing is required to get a complete phase separation and recrystallization of the Si overlayer.

Acknowledgements

The research support of the Spanish CICYT Contract No. MAT98-0823 is gratefully acknowledged. One of the authors, L. Barbadillo, would like to thank the support of the Comunidad de Madrid under a FPI grant. We thank C.J. Pastor for his technical assistance in XRD measurements. TEM measurements were performed at the "División de Microscopía Electrónica de la Universidad de Cádiz".

References

[1] A.R. Powell, S.S. Yyer, F.K. LeGoues, Appl. Phys. Lett. 64 (1994) 1856.
[2] J.B. Lin, S.S. Yyer, J. Min, P.K. Chun, R. Gronsky, C. Hu, N.W. Cheung, in: J. Schrankles (Ed.), IEEE International SOI Conference proceedings, IEEE, New York, 1995, p. 166.
[3] M. Bruel, Nucl. Instr. and Meth. B 108 (1996) 313.
[4] Q.-Y. Tong, T.-H. Lee, K. Gutjahr, S. Hopfe, V. Gösele, Appl. Phys. Lett. 70 (1997) 1390.
[5] D. Teng, Y.H. Lo, Appl. Phys. Lett. 62 (1993) 43.
[6] L.B. Freund, W.D. Nix, Appl. Phys. Lett. 69 (1996) 173.
[7] C.M.S. Rauthan, J.K. Srivastava, Mater. Lett. 9 (1990) 252.
[8] N. Hatzopoulos, V. Bussmann, A.K. Robinson, P.L.F. Hemment, Nucl. Instr. and Meth. B 55 (1991) 734.
[9] L. Chenglu, L. Jinghua, Z. Shunkai, Y. Yuchui, Z. Shickang, Nucl. Instr. and Meth. B 55 (1991) 742.
[10] S.W. Polchlopek, G.H. Bernstein, R.Y. Kwor, IEEE Trans. Electron. Dev. 40 (1993) 385.
[11] A. Södebärg, J. Electrochem. Soc. 139 (1992) 561.
[12] A. Pérez-Rodríguez, A. Romano-Rodríguez, J.R. Morante, M.C. Acero, J. Esteve, J. Montserrat, A. El-Hassani, J. Electrochem. Soc. 143 (1996) 1026.
[13] S. Wolf, Silicon Processing for the VLSI Era, Vol. 3, Lattice Press, CA, 1995, p. 330.
[14] D. Wang, Y. Hiroyama, M. Tamura, M. Ichikawa, Appl. Phys. Lett. 76 (1993) 1683.
[15] L. Frey, J. Stoemenos, R. Schork, A. Nejim, P.L.F. Hemment, J. Electrochem. Soc. 144 (12) (1997) 4314.
[16] A. Nakao, M. Iwaki, H. Sakairi, K. Terasima, Nucl. Instr. and Meth. B 65 (1992) 352.
[17] S. Miyagawa, S. Nakao, K. Saitoh, M. Ikeyama, H. Niwa, S. Tanemura, Y. Miyagawa, K. Baba, J. Appl. Phys. 78 (12) (1995) 7018.
[18] F.J. Gómez, P. Prieto, E. Elizalde, J. Piqueras, Appl. Phys. Lett. 69 (6) (1996) 773.
[19] L. Barbadillo, F.J. Gómez, M.J. Hernández, J. Piqueras, Appl. Phys. A 68 (1999) 603.
[20] L.C. Chen, C.K. Chen, S.L. Wei, D.M. Bhusari, K.H. Chen, Y.F. Chen, Y.C. Jong, Y.S. Huang, Appl. Phys. Lett. 72 (19) (1998) 2463.
[21] J.F. Ziegler, SRIM Program, copyright IBM-Research, Yorktown, NY, 1996.
[22] S. Isomae, T. Ishiba, T. Ando, M. Tamura, J. Appl. Phys. 74 (1993) 3815.
[23] C. Serre, A. Pérez-Rodríguez, A. Romano-Rodríguez, J.R. Morante, R. Kögler, W. Skorupa, J. Appl. Phys. 77 (1995) 2978.
[24] E. Theodossiu, H. Baumann, K. Bethge, J. Appl. Phys. 86 (8) (1999) 4703.
[25] M.A. El Khakani, M. Chaker, M.E. O'Hern, W.C. Oliver, J. Appl. Phys. 82 (9) (1997) 4310.
[26] F.J. Gómez, J. Martínez, J. Garrido, C. Gómez-Aleixandre, J. Piqueras, J. Non-Cryst. Solids 191 (1995) 164.
[27] F.J. Gómez, J. Garrido, J. Martínez, J. Piqueras, J. Electrochem. Soc. 143 (1) (1996) 271.
[28] G. Spitzer, D.A. Kleiman, D. Walsh, Phys. Rev. 113 (1959) 127.
[29] D. Chen, W.Y. Cheung, S.P. Wong, Nucl. Instr. and Meth. B 148 (1999) 589.
[30] S.P. Wong, D. Chen, L.C. Ho, H. Yan, R.W.M. Kwok, Nucl. Instr. and Meth. B 140 (1998) 70.

[31] T.O. Mitchell, J.L. Hoyt, J.F. Gibbons, Appl. Phys. Lett. 71 (12) (1997) 1688.
[32] E.A. Taft, J. Electrochem. Soc. 118 (1971) 1341.
[33] V.I. Belyi, L.L. Vasilyeva, A.S. Ginovker, V.A. Gritsenko, S.M. Repinsky, S.P. Sinitsa, T.P. Smirnova, F.L. Edelman, in: Material Science Monographs Silicon Nitride in Electronics, Elsevier, Amsterdam, 1988, p. 138.
[34] L. Barbadillo, M.J. Hernández, M. Cervera, P. Rodríguez, J. Piqueras, J. Appl. Phys. 87 (2000) 8201.
[35] R.M. Azzam, N.M. Bashara, Ellipsometry and Polarized Light, North-Holland, Amsterdam, 1987.
[36] D.E. Aspnes, J.B. Theeten, J. Appl. Phys. 50 (1979) 4928.
[37] W.J. Choyke, E.D. Palik, in: E.D. Palik (Ed.), Handbook of Optical Constants of Solids, Academic Press, New York, 1985, p. 587.
[38] H.G. Tompkins, A User's Guide to Ellipsometry, Academic Press, New York, 1993, p. 246.